RESEARCH ARTICLE

WILEY

Probabilistic analysis of strip footings based on enhanced Kriging metamodeling

Abdul-Kader El Haj[1] | Abdul-Hamid Soubra[1] | Tamara Al-Bittar[2]

[1] Institut de Recherche en Génie Civil et Mécanique (GeM), University of Nantes, Saint-Nazaire, France

[2] Lebanese University, Faculty of Engineering, Branch I, Haykaliyeh, Al Koura, Lebanon

Correspondence
Abdul-Kader El Haj, Institut de Recherche en Génie Civil et Mécanique (GeM), University of Nantes, Bd. de l'Université, 44603 Saint-Nazaire, France.
Email: abdul-kader.el-haj@etu.univ-nantes.fr

Summary

Two advanced Kriging metamodeling techniques were used to compute the failure probability of geotechnical structures involving spatially varying soil properties. These methods are based on a Kriging metamodel combined with a global sensitivity analysis that is called in literature Global Sensitivity Analysis-enhanced Surrogate (GSAS) modeling for reliability analysis. The GSAS methodology may be used in combination with either the Monte Carlo simulation (MCS) or importance sampling (IS) method. The resulting Kriging metamodeling techniques are called GSAS-MCS or GSAS-IS. The objective of these techniques is to reduce the number of calls of the mechanical model as compared with the classical Kriging-based metamodeling techniques (called AK-MCS and AK-IS) combining Kriging with MCS or IS. The soil uncertain parameters were assumed as non-Gaussian random fields. EOLE methodology was used to discretize these random fields. The mechanical models were based on numerical simulations. Some probabilistic numerical results are presented and discussed.

KEYWORDS

Kriging, probabilistic analysis, random fields, spatially varying soil, strip footing

1 | INTRODUCTION

This paper focuses on the computation of the failure probability of geotechnical structures involving spatially varying soil properties. When performing a probabilistic analysis of these structures, the system response is generally related to the system inputs by finite element/finite difference simulations that may be computationally-expensive. This impedes the computation of the small practical values of the failure probability by Monte Carlo Simulation (MCS) methodology. Indeed, the computation of a small value of the failure probability by MCS requires a huge number of simulations. For instance, 10^{n+2} simulations are required to compute a failure probability of 10^{-n} for a coefficient of variation on the failure probability of 10%. In order to overcome the shortcoming of a large number of simulations, some authors have resorted to more efficient probabilistic methods called "variance reduction techniques" (eg, Ahmed and Soubra,[1] Yuan et al,[2] Li et al,[3] Jiang and Huang,[4] Li et al,[5] Xiao et al,[6] Huang et al,[7] Jiang et al,[8] and Van Den Eijnden and Hicks[9]). Although the variance reduction techniques are powerful probabilistic approaches, they remain insufficient when dealing with a small value of the failure probability and a small desired value of the coefficient of variation on this failure probability. Consequently, more advanced probabilistic approaches requiring a smaller number of simulations (ie, a smaller number of calls to the mechanical model) were needed.

During the last few decades, some metamodeling techniques were developed in literature such as the polynomial chaos expansion (PCE), the Kriging method, the support vector machine (SVM), the artificial neural networks (ANN), and the response surface method (RSM). The basic idea of a metamodeling technique is to replace the response of the mechanical model (which may be computationally-expensive) by a metamodel (ie, a simple analytical equation) using a small number of evaluations of the system response. More recently, various advanced probabilistic approaches combining a metamodeling technique with a simulation method (eg, MCS, IS, or subset simulation [SS]) have been reported in literature. For instance, Bourinet et al[10] proposed a method combining subset simulation and support vector machines, Dubourg et al[11] suggested a combination between subset simulation and Kriging, and Echard et al[12,13] combined Kriging metamodeling with Monte Carlo and importance sampling, respectively. All these methods take advantage of both the metamodeling and the simulation techniques. They aim at efficiently computing the small failure probabilities on the basis of the constructed metamodel, making use of a reduced number of calls to the time-demanding mechanical model.

This paper takes benefit from the two methods developed by Echard et al.[12,13] These methods are, respectively, the Active learning method combining Kriging and MCS (named AK-MCS method) and the Active learning method combining Kriging and IS (named AK-IS method). Notice that both AK-MCS and AK-IS approaches involve the construction of a surrogate Kriging metamodel on the basis of the responses of a small design of experiments (DoE) computed using the mechanical model. This approximate Kriging metamodel is then successively updated *via* an enrichment process by selecting new training samples that are close to the limit state surface. The strategy of selection of a new training sample is based on a powerful learning function that takes benefits from the Kriging characteristics. Once the adopted convergence criterion indicates that the Kriging model is sufficiently improved, MCS methodology is applied on the obtained Kriging surrogate model instead of the time-consuming mechanical model. It should be emphasized here that the aim of the constructed metamodel is not to determine the accurate values of the performance function for the different samples but rather to accurately determine the signs of the performance function values for these samples in order to accurately compute the probability of failure.

As was stated by Hu and Mahadevan,[14] the essential issues in AK-MCS and AK-IS lie in (a) the choice of a "best" new training sample during the enrichment process and (b) the stopping criterion related to the addition of a new training sample. Indeed, the strategy of selection of a new training sample and the convergence criterion are defined on the basis of the individual responses at the different Monte Carlo population samples. This may lead to some extra evaluations of unnecessary new training samples.

In order to overcome the shortcomings of AK-MCS and AK-IS approaches for the reliability analysis, a global sensitivity analysis-enhanced surrogate (GSAS) modeling was developed by Hu and Mahadevan.[14] This methodology is used in this paper. It is based on a Kriging metamodel combined with a global sensitivity analysis. Two techniques called GSAS-MCS and GSAS-IS were proposed within GSAS methodology. These techniques combine GSAS with either MCS or IS. Within GSAS methodology, both the strategy of selecting new training samples and the convergence criterion are defined from the perspective of reliability estimate (ie, they are based on the failure probability estimate which represents the quantity of interest for the probabilistic analysis) instead of focusing on the individual responses at the different Monte Carlo samples. Indeed, the new training samples are identified according to their contribution to the uncertainty in the estimated failure probability $\widehat{P}_f$ (based on a global sensitivity analysis), and the selection of new training samples stops when the accuracy of the estimated $\widehat{P}_f$ reaches a specific target.

It should be mentioned that Hu and Mahadevan[14] have validated the proposed GSAS methodology on the basis of several academic examples for which the performance function was given by an analytical equation (ie, where the computation time of the corresponding performance function is quasi-negligible). A significant reduction in the number of calls to the performance function has been obtained when using GSAS methodology, as compared with the classical Kriging-based methodology by Echard et al.[12]

The aim of this paper is to extend the GSAS methodology proposed by Hu and Mahadevan[14] to the case of random field problems in order to study geotechnical structures involving spatial variability of the soil properties. More specifically, GSAS-MCS and GSAS-IS techniques are used in this paper for the computation of the failure probability of shallow foundations resting on a spatially varying soil. Two problems involving ultimate and serviceability limit states are considered. These problems are quite time-consuming because the corresponding mechanical models used for the computation of the performance function are based on numerical simulations.

This paper is organized as follows: Section 2 presents the problem definition. In Section 3, the GSAS general procedure as adapted to the case of geotechnical structures involving spatially varying soil properties is presented—both GSAS-MCS and GSAS-IS techniques are described in some details. In Section 4, some numerical probabilistic results are presented and discussed. The paper ends by a conclusion of the main findings in Section 5.

2 | PROBLEM DEFINITION

Two geotechnical problems based on numerical simulations using FLAC[3D] finite difference code and involving ultimate and serviceability limit states were considered in this paper.

The first problem aims at performing a probabilistic analysis at the ultimate limit state (ULS) of a strip footing resting on a one-layer spatially varying soil medium and subjected to a vertical load. The objective is the computation of the probability P_f against soil punching. This problem was recently considered by Pieczyńska-Kozłowska et al[15] using the random finite element method (RFEM) (cf. Griffiths & Fenton,[16] Griffiths et al,[17] and Fenton & Griffiths[18]). The numerical model considered in the present analysis consists of a strip footing of breadth B = 1 m, which rests on a soil domain of width 13B and depth 5B (cf. Figure 1). The length of the largest element of the deterministic mesh in a given direction (horizontal or vertical) was chosen in this paper such that it does not exceed 0.5 times the autocorrelation distance in that direction.[19] The soil behavior was modeled using a conventional elastic, perfectly plastic model on the basis of the Mohr-Coulomb failure criterion. The soil cohesion c and angle of internal friction φ were modeled as two anisotropic non-Gaussian random fields. The soil dilation angle ψ was considered to be related to the soil angle of internal friction φ by $\psi = 2\,\varphi/3$. This means that the soil dilation angle was implicitly assumed as a random field that is perfectly correlated to the soil angle of internal friction random field. The illustrative statistical parameters of the two random fields c and φ as used in the present paper are provided in Table 1. Concerning the soil elastic parameters, the soil Young modulus E and Poisson ratio υ were considered as deterministic parameters in this problem with the following values: $E = 60$ MPa and $\upsilon = 0.3$. The footing is subjected to an applied load $q_s = 400$ kN/m. The ultimate deterministic footing load computed by FLAC[3D] using the mean values of the soil shear strength parameters is equal to 1,190 kN/m. This corresponds to a safety factor against soil punching of about 3.0. Although the present analysis focuses on a single layer soil medium, the present probabilistic approaches may be extended to the case of spatially varying multi-layered soil medium by using numerical simulations from finite element method or by employing numerical limit analysis simulations as those presented by Eshkevari et al.[20]

The second geotechnical problem aims at performing a probabilistic analysis at the serviceability limit state (SLS) of two neighboring strip footings resting on a spatially varying soil and subjected to central vertical loads with equal magnitude. The objective in this problem is to compute the failure probability against exceeding a prescribed threshold on the differential settlement between the two footings. The numerical model consists of two footings of breadth b = 2 m, which rest on a soil domain of width 9b and depth 3b (cf. Figure 2). The two footing centers are separated by a distance equal to 4 m. Each footing is subjected to a central vertical load of 1,000 kN/m. An optimized non-uniform symmetrical mesh was adopted (cf. Figure 2). As before, the length of the largest element in a given direction was chosen such that it does not exceed half the value of the autocorrelation distance in that direction.[20] Concerning the soil behavior, it was modeled in this problem using the conventional elastic-perfectly plastic model based on the Mohr-Coulomb failure criterion in order to take into account the possible plastification that may take place near the footings edges even under service load conditions. In this SLS problem, the soil Young modulus E was modeled as an anisotropic non-Gaussian random field. A lognormal distribution was used for E with a mean value of 60 MPa and a coefficient of variation of 15%. The randomness of the Poisson ratio was neglected, and a deterministic value of 0.3 was adopted. The soil shear strength parameters were also considered as deterministic parameters in this problem with the following values: $c = 20$ kPa, $\varphi = 30°$, and $\psi = 2\,\varphi/3$.

It should be noted that the same square exponential autocorrelation function was used for all the random fields considered in this paper (ie, c, φ, and E). This autocorrelation function is given by the following equation:
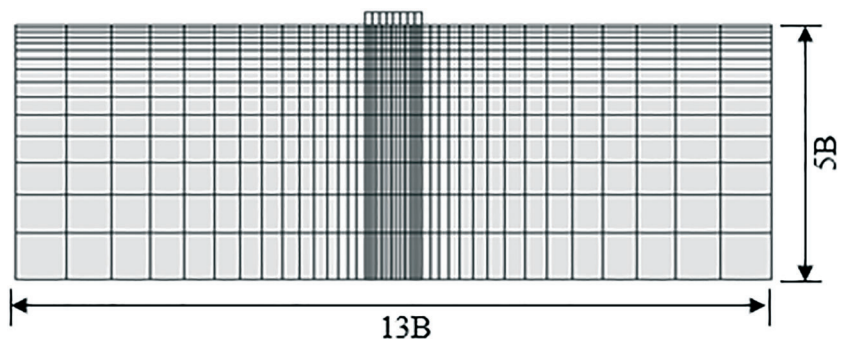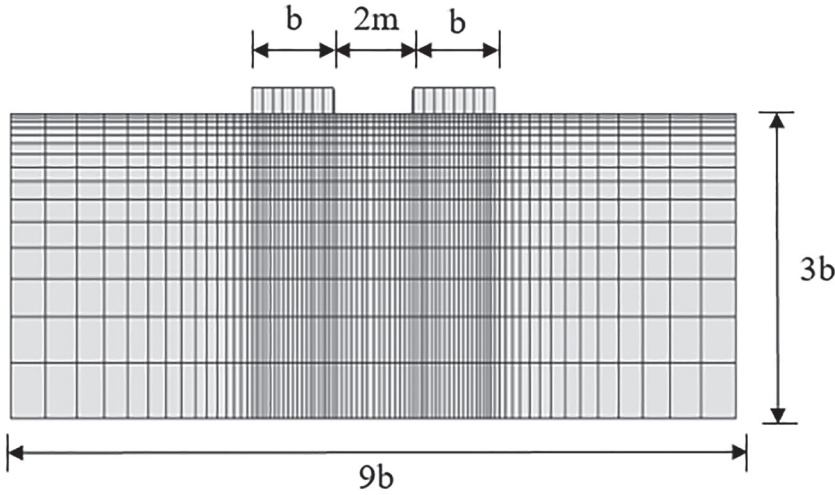

FIGURE 1 Soil domain and mesh used in the numerical simulations for the soil punching problem

TABLE 1 Statistical characteristics of the random fields

Random Field	Mean, μ	Coefficient of variation COV, %	Type of the Probability Density Function (PDF)
c	20 kPa	25	Log-normal
φ	30°	10	Beta

FIGURE 2 Soil domain and mesh used in the numerical simulations for the differential settlement problem

$$\rho = \exp\left(-\left(\frac{|\Delta x|}{a_x}\right)^2 - \left(\frac{|\Delta y|}{a_y}\right)^2\right), \tag{1}$$

where a_x and a_y are the autocorrelation distances along x and y, respectively. Notice also that the values of the autocorrelation distances considered in this paper will be given later when dealing with the numerical results.

The EOLE methodology suggested by Li and Der Kiureghian[21] was used in this paper to discretize the random fields (ie, to obtain realizations of the soil properties that respect the correlation structure of those fields). This method allows one to compute the variance of the error of the corresponding discretization scheme and thus, to determine the minimal (optimal) number M of eigenmodes that is required for a prescribed value of the variance of the error. It should be noted that the discretization of a random field by EOLE leads to an expression that provides the value of this random field at each point of the soil mass as a function of M standard Gaussian random variables (this number M is equal to the number of eigenmodes). For a prescribed value of the variance of the error on EOLE, the number M is small for the high values of the autocorrelation distances (ie, case of a homogeneous soil) and it increases with the decrease of the autocorrelation distance.

3 | GSAS GENERAL PROCEDURE FOR SOIL SPATIAL VARIABILITY PROBLEMS

The extension of the GSAS approach by Hu and Mahadevan[14] to the case of spatially varying soil properties is presented in some details in this section. Firstly, the GSAS-MCS technique (which may be considered as an improvement of AK-MCS) is presented. Then, the GSAS-IS technique based on IS instead of MCS will be briefly described.

Before the presentation of GSAS-MCS and GSAS-IS approaches, it should be noted that the Kriging technique allows one to construct a metamodel (ie, an analytical model) on the basis of a few number of samples (ie, a small DoE) computed using the mechanical model. According to the Kriging property, the predicted response at an unknown sample $x^{(i)}$ (as determined on the basis of the constructed Kriging surrogate model) is a random Gaussian variate as follows:

$$G_p\left(x^{(i)}\right) \sim N\left(\widehat{g}\left(x^{(i)}\right), \sigma_{G_p}^2\left(x^{(i)}\right)\right),$$

where N stands for the Normal distribution, $\widehat{g}\left(x^{(i)}\right)$ and $\sigma_{G_p}^2\left(x^{(i)}\right)$ are the Kriging mean prediction and the corresponding mean square error (prediction variance), respectively. The variances of the samples in the DoE are zero, but the

variances of the other samples are always different from zero. For more details concerning the theory of Kriging metamodeling, the reader may refer to Sacks et al[22] or to different recently published papers using Kriging metamodeling as in Echard et al[12,13] and Al-Bittar et al.[23]

3.1 | GSAS-MCS technique

The GSAS-MCS technique as adapted to the case of random field problems can be summarized by the two following stages:

3.1.1 | Stage 1 (construction of a preliminary Kriging metamodel)

This stage includes three steps:

1. In step 1, one generates a large Monte Carlo population $x^{(i)}$ ($i = 1,2,...,N_{MCS}$), where N_{MCS} was taken equal to 500 000 samples. Each sample is composed of M standard Gaussian random variables where M is the number of random variables (or the number of eigenmodes), which is needed by EOLE methodology to obtain a variance of the error that is smaller than a target prescribed value as was explained in the previous section. In this paper, a target maximal value of 5% was imposed for the variance of the error by EOLE methodology as it may be seen from the third column of Table 4.
2. In step 2, one randomly selects a small design of experiments DoE from the generated population (a DoE of 20 samples was used in this work) and then, one computes for each sample, the realizations (ie, typical spatial variations) of the random fields (ie, c and φ in the first geotechnical problem and E in the second geotechnical problem) on the basis of EOLE methodology. For each selected sample, one should also compute the performance function G that is defined by Equation (2) for the first geotechnical problem and by Equation (3) for the second problem.

$$G = \frac{q_u}{q_s} - 1, \tag{2}$$

$$G = \delta_{max} - \delta. \tag{3}$$

In Equation (2), q_u represents the ultimate bearing capacity computed on the basis of FLAC^{3D} software, making use of the obtained realizations of c and φ, and q_s is the footing applied loading. In Equation (3), δ represents the value of the differential settlement computed using the obtained realization of E, and δ_{max} is the prescribed threshold on the differential settlement. The value of δ_{max} was assumed to be equal to 3×10^{-3} m in this paper. For both equations (ie, Equations 2 and 3), a negative (respectively positive) value of G indicates that the considered realization is located in the failure (respectively safe) domain.
   On the basis of the DoE and the corresponding performance function evaluations, one should construct an approximate Kriging metamodel in the standard space of random variables using the DACE toolbox.[24]
3. In step 3, one should determine the Kriging predictions values $\widehat{g}\left(x^{(i)}\right)$ (ie, mean values) and their corresponding Kriging prediction variances $\sigma^2_{G_p}\left(x^{(i)}\right)$, for the whole MCS samples, using the DACE toolbox. The estimated failure probability $\widehat{P}_f$ may be computed using the following equation:

$$\widehat{P}_f = \sum_{i=1}^{N_{MCS}} I\left(G_p\left(x^{(i)}\right)\right)/N_{MCS}, \tag{4}$$

where the metamodel random responses $G_p(x^{(i)})$ in this equation are replaced by the mean prediction values $\widehat{g}\left(x^{(i)}\right)$. Notice that in Equation (4), $I(G_p(x^{(i)})) = 1$ if $G_p(x^{(i)}) \leq 0$; otherwise, $I(G_p(x^{(i)})) = 0$, where $x^{(i)}(i = 1,2,...,N_{MCS})$ is the Monte Carlo population. Thus, $\widehat{P}_f$ is estimated by counting the number of negative mean predictors and dividing it by the total number of MCS samples. The corresponding coefficient of variation $COV\left(\widehat{P}_f\right)$ is given by the following equation:

$$COV\left(\widehat{P}_f\right) = \sqrt{\frac{1 - \widehat{P}_f}{\widehat{P}_f . \, N_{\mathrm{MCS}}}}. \qquad (5)$$

It should be emphasized here that the value of the failure probability computed at this stage is far from being accurate because of the small DoE used so far. An enrichment process is thus needed.

3.1.2 | Stage 2 (enrichment process)

According to the property of the Kriging metamodeling, the predicted responses $G_p(x^{(i)})$ are random variates presenting some uncertainty. Hence, the failure probability estimate $\widehat{P}_f$ given by Equation (4) is also a random variate since it is a sum of random variates. The variance in the failure probability estimate $\widehat{P}_f$ is given by the following equation (see Hu and Mahadevan[14]):

$$Var\left(\widehat{P}_f\right) \approx \frac{1}{N_{MCS}^2}\left(\sum_{i=1}^{N_{MCS}} Var\left(I\left(G_p\left(\boldsymbol{x}^{(i)}\right)\right)\right) + \sum_{i \neq j} Cov\left(I\left(G_p\left(\boldsymbol{x}^{(i)}\right)\right), I\left(G_p\left(\boldsymbol{x}^{(j)}\right)\right)\right)\right), \qquad (6)$$

where the first summation represents the sum of the individual variances of the predicted responses and the second one represents the sum of the covariances between these responses.

Within AK-MCS and AK-IS approaches, the best next candidate sample adopted during the enrichment process is selected as the one that has the highest probability of being misclassified with respect to the sign of its performance function value. This choice aims at reducing the individual variances coming from the first part of Equation (6), but it does not consider the effect of the correlation between samples (second part of Equation 6) on the uncertainty of $\widehat{P}_f$. Furthermore, the convergence criterion adopted in AK-MCS (or AK-IS) approach is defined from the aspect of individual samples (ie, when all the individual variances of the different MCS [or IS] samples are reduced) but not from the aspect of the reliability estimate accuracy. The GSAS methodology allows one to overcome this shortcoming.

The basic idea of GSAS is to treat the probability of failure estimate $\widehat{P}_f$ as a random variate representing the output of the system presented in Figure 3 where the system inputs are the random responses $G_p(x^{(i)})$ predicted by the Kriging metamodel.

Strategy of selecting a new training sample
For an efficient enrichment of the Kriging metamodel, the new training sample is selected within GSAS on the basis of its contribution to the uncertainty of the quantity of interest (ie, $\widehat{P}_f$). This is done *via* a global sensitivity analysis method
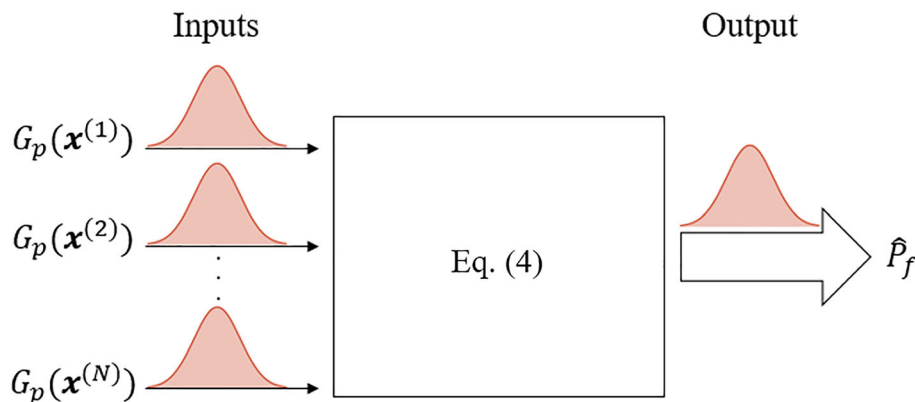

FIGURE 3 Probability of failure estimate as a system response (after Hu & Mahadevan, 2016) [Colour figure can be viewed at wileyonlinelibrary.com]

extended to the case of models with dependent inputs. The extended FAST method developed by Xu and Gertner[25] was used in this paper. The enrichment process within GSAS approach can be briefly described as follows:

The MCS samples $x^{(i)}(i = 1, 2, ..., N_{MCS})$ are divided into two groups: (a) group x_{g1}^{MCS} where the different samples have U values that are larger than 2 and (b) group x_{g2}^{MCS} with the remaining samples, U being a classical learning function that is usually employed in the Kriging-based approaches (see Echard et al[12,13]). It is given by:

$$U\left(x^{(i)}\right) = \frac{\left|\widehat{g}\left(x^{(i)}\right)\right|}{\sigma_{G_p}\left(x^{(i)}\right)}. \tag{7}$$

Samples with a value of U that is larger than 2 are considered to have at most a probability of about 2.5% of being misclassified (ie, a very small probability to have wrong performance function signs) as was shown by Echard et al.[12]

The global sensitivity analysis is then performed on the samples of the x_{g2}^{MCS} group to determine their contributions to the uncertainty of $\widehat{P}_f$ since we assume that the uncertainty of $\widehat{P}_f$ comes from this group of samples. It should be noted that in order to reduce the dimensionality of the problem, only a reduced number n_{can} of samples (taken equal to 20 in this work) of the x_{g2}^{MCS} group with the lowest U values are selected to perform the global sensitivity analysis since they have the highest probabilities of having wrong performance function signs (ie, high probability of being the new selected training sample). Finally, the sample having the biggest contribution to the uncertainty of $\widehat{P}_f$ is selected to be evaluated and to be used for the enrichment process. Notice that the number of samples in group x_{g1}^{MCS} is denoted in this paper by N_1 and that of group x_{g2}^{MCS} is denoted by N_2. Notice also that the number N_1 is expected to increase and the number N_2 is expected to decrease during the enrichment process because of the successive improvement of the metamodel during this process.

Stopping condition

A powerful stopping criterion based on the quantification of the uncertainty in the failure probability was suggested within GSAS methodology (cf. Hu and Mahadevan[14]). These authors suggest stopping the addition of new samples based on the uncertainty of the error on the failure probability ε_r. The error on the failure probability is a measure of the gap between the theoretical and the computed values of the failure probability. It is defined by the following equation:

$$\varepsilon_r = \frac{\widehat{P}_f - \widehat{P}_f^{'}}{\widehat{P}_f}, \tag{8}$$

where $\widehat{P}_f$ is the theoretical failure probability given by Equation (4) and $\widehat{P}_f^{'}$ is its estimated value that can be directly computed by replacing the Kriging metamodel random responses $G_p(x^{(i)})$ by the mean prediction values $\widehat{g}\left(x^{(i)}\right)$.

It should be noted here that $\widehat{P}_f$ in Equation (8) is a random variate since it is a function of the Kriging predictions that are random normal variates (according to the Kriging property as was stated before). Thus, the error ε_r as given by Equation (8) is also a random variate for which one may quantify the corresponding uncertainty on the basis of the uncertainty quantification of $\widehat{P}_f$. To do this, the sampling-based method was used as follows:

This method consists in generating n_r samples ($n_r = 600$ in this paper), where each sample is composed of N_2 normal variables $G_p\left(x_{g2}^{MCS}(i)\right)$, $i = 1, 2, ..., N_2$; N_2 being the number of samples in the x_{g2}^{MCS} group. From these samples, one can compute n_r samples of the failure probability $\widehat{P}_f$ and then n_r corresponding samples of the error ε_r. From the obtained samples $\varepsilon_r(i), i = 1, 2, ..., n_r$, the Kernel smoothing function is employed to fit the distribution of ε_r. On the basis of the fitted distribution, Hu and Mahadevan[14] have suggested stopping the addition of new samples when the quantity ε_r^{max} becomes smaller than a prescribed threshold a (a is taken equal to 0.1% in this paper), where ε_r^{max} is defined as follows:

$$\varepsilon_r^{max} = \max\left\{\left|F_{\varepsilon_r}^{-1}(0.99)\right|, \left|F_{\varepsilon_r}^{-1}(0.01)\right|\right\}. \tag{9}$$

In this equation, $F_{\varepsilon_r}^{-1}$ is the inverse CDF of ε_r. The proposed stopping condition corresponds to a probability that the actual estimation error on $\widehat{P}_f$ is larger than 0.1%, is equal to 0.02. In other words, this criterion ensures a very small possibility of having a relatively big error on the estimation of $\widehat{P}_f$.

Notice finally that the value of $\varepsilon_r^{\max}$ was checked every time the surrogate model was updated, except for the case where the number N_2 was still too large (more than 8,000 samples in this paper). The reason is related to the fact that the error computation cost is very expensive in this case. Furthermore, this cost would be with no interest since the uncertainty on the failure probability estimate is obviously significant in the case where the number N_2 of samples in the group x_{g2}^{MCS} is large. Remember here that the uncertainty in the failure probability was assumed to come from the x_{g2}^{MCS} group.

3.2 | GSAS-IS technique

This section presents the combination between GSAS methodology and the IS variance reduction technique. Such a combination (called GSAS-IS technique) serves in reducing the samples population size with respect to GSAS-MCS, while conserving the small value of the coefficient of variation on the failure probability. Notice that a reduction in the samples population size (eg, 10 000 samples in GSAS-IS instead of 500 000 samples in GSAS-MCS) has the advantage of reducing the number of metamodel predictions for each enrichment iteration and thus, a reduction in the corresponding computation time.

The GSAS-IS procedure (as adapted to the case of random fields) consists of two main stages. In the first stage, the most probable failure point (design point) is determined *via* an iterative procedure using an approximate Kriging metamodel based on a small number of samples. In the second stage, the obtained approximate Kriging metamodel is successively improved *via* an enrichment process (as in GSAS-MCS). Notice however that in GSAS-IS, the enrichment is performed based on samples generated according to the probability density function of a multivariate Gaussian distribution that is shifted to the obtained design point.

The step-by-step procedure of the GSAS-IS method is nearly the same as that of GSAS-MCS described in Section 3.1. The differences involve step (3) of stage 1 and the sampling by IS (instead of MCS) during the enrichment process.

Step (3) of stage 1 within GSAS-IS can be described as follows (steps a to d):

a. Find the minimum value of the Hasofer-Lind reliability index and the corresponding design point by making use of the approximate already-obtained Kriging metamodel for the performance function. This procedure gives an approximate value of the reliability index and its corresponding design point.

b. Generate a small number of samples (five samples are used in this paper) of M standard Gaussian random variables. Then, translate these samples such that the obtained samples follow a shifted multivariate Gaussian distribution having a mean vector whose components are equal to the coordinates of the obtained design point in the standard coordinate system. After the generation of the five samples, transform each sample into realization(s) of the random field(s). Finally, for each one of the five samples, compute the corresponding value of the performance function using FLAC$^{\mathrm{3D}}$.

c. Construct a new Kriging metamodel in the standard space using all samples generated so far. This Kriging metamodel is used to obtain an updated design point and its corresponding Hasofer-Lind reliability index.

d. Steps b and c are repeated several times until the absolute difference between two successive values of the Hasofer-Lind reliability index becomes smaller than a given tolerance (taken equal to 0.01).

It should be noted here that steps a to d described above were suggested in Soubra et al.[26] They were applied within this paper because we are dealing here with an analytically unknown performance function. These steps were not needed in the paper by Hu and Mahadevan[14] because only analytical performance functions were considered by these authors.

Concerning the enrichment process, once the final design point is obtained, an IS population (with a reduced number of samples of say 10 000 samples) is generated according to the PDF of a multivariate Gaussian distribution shifted to the obtained design point. The failure probability estimate $\widehat{P}_f$ is calculated using the following formula of importance sampling approach:

$$\widehat{P}_f = \frac{1}{N_{\mathrm{IS}}} \sum_{i=1}^{N_{\mathrm{IS}}} I\left(G_p\left(x^{(i)}\right)\right) \frac{f\left(x^{(i)}\right)}{h(x^{(i)})}, \tag{10}$$

in which $I(G_p(x^{(i)}))$ is the indicator function, $I(G_p(x^{(i)})) = 1$ when $G_p(x^{(i)}) \leq 0$ and $I(G_p(x^{(i)})) = 0$ when $G_p(x^{(i)}) > 0$; $f(x^{(i)})$ is the PDF of the initial multivariate standard Gaussian distribution; $h(x^{(i)})$ is the PDF of the shifted multivariate

Gaussian distribution; and N_{IS} is the number of samples in IS. The coefficient of variation $COV\left(\widehat{P}_f\right)$ is given by the following equation:

$$COV\left(\widehat{P}_f\right) = \frac{\sqrt{Var\left(\widehat{P}_f\right)}}{\widehat{P}_f}, \tag{11}$$

where $Var\left(\widehat{P}_f\right)$ is the variance of the failure probability estimate. It is calculated by the following equation:

$$Var\left(\widehat{P}_f\right) = \frac{1}{N_{IS}-1}\left[\frac{1}{N_{IS}}\sum_{i=1}^{N_{IS}}\left(I\left(G_p\left(x^{(i)}\right)\right)\left(\frac{f\left(x^{(i)}\right)}{h\left(x^{(i)}\right)}\right)^2\right) - \widehat{P}_f^2\right]. \tag{12}$$

It should be emphasized herein that the enrichment process is similar to that of GSAS-MCS, except that the selection of the enrichment samples is done among the reduced IS population (10 000 samples). Notice also that the number N_2 is considered herein as being too large if it is bigger than 1000 samples.

4 | NUMERICAL RESULTS

4.1 | Probabilistic results of the soil punching problem

In this section, the failure probability against soil punching of a strip footing resting on a spatially varying soil is computed. Both GSAS-MCS and GSAS-IS techniques are used for the computations. The results provided by the proposed techniques are compared with those obtained by employing the classical Kriging-based approaches (ie, AK-MCS and AK-IS). A reference practical configuration with a vertical autocorrelation distance of 2 m and a horizontal autocorrelation distance of 10 m was considered in this section. For this case, 18 random variables were adopted within EOLE methodology with a corresponding value of the variance of the error of 4.1%. Such a small value of the error (smaller than 5%) indicates a sufficiently accurate random field discretization.

4.1.1 | GSAS probabilistic results

Figure 4 shows the evolution of the error ε_r^{max}, with the number of added samples during the enrichment process as obtained when using GSAS-MCS. Similar trend was obtained when using GSAS-IS (figure not shown). It should be noted that the error ε_r^{max} was not computed before reaching 52 added samples because of the high uncertainty in the

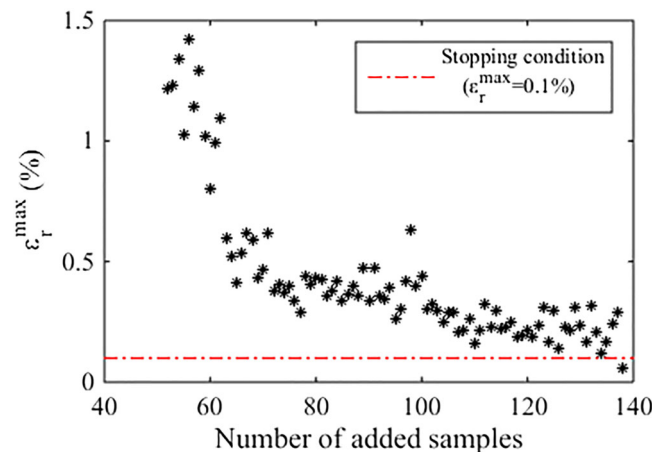**FIGURE 4** ε_r^{max} vs the number of added samples within GSAS-MCS when $a_x = 10$ m and $a_y = 2$ m [Colour figure can be viewed at wileyonlinelibrary.com]

failure probability estimate (indicated by the large value of $N_2 > 8000$ as was mentioned before) and the corresponding high computation cost. Beyond 52 added samples, ε_r^{max} was computed each time a new sample was added during the enrichment process until reaching the stopping condition ($\varepsilon_r^{max} < 0.1\%$) shown by the horizontal dotted red line. This criterion has led to a number of added samples equal to 138 as shown in Figure 4.

Figure 5 shows the decreasing trend of the number N_2 of samples of x_{g2}^{MCS} group with the increase in the number of added samples. The number N_2 of samples was shown to be important ($N_2 = 115\,677 > 8000$ samples) at the beginning of the enrichment process when the metamodel was still not updated. This number decreases with the increase in the number of added samples. When N_2 has become below 8000 samples (which corresponds to a number of added samples that is larger than 52), the computation of ε_r^{max} was undertaken until reaching the stopping condition ($\varepsilon_r^{max} < 0.1\%$). This criterion was satisfied for 138 added samples. At this point, N_2 was found to be equal to 1803. A further decrease in the number N_2 was not necessary because the stopping criterion was satisfied. It should be emphasized here that the number N_2 in AK-MCS is equal to zero at the end of the enrichment process since the corresponding stopping criterion requires that all the samples of the MCS population have a U value that is greater than 2.

Figure 6 presents the distribution of ε_r for three different numbers of added samples as obtained from GSAS-MCS method. Similar trend was obtained from GSAS-IS method (figure not shown). This figure shows that the variability of ε_r decreases with the number of added samples. When reaching the optimal number of added samples (ie, 138 samples), the mean value of the error converges to zero and the corresponding value of the standard deviation becomes very
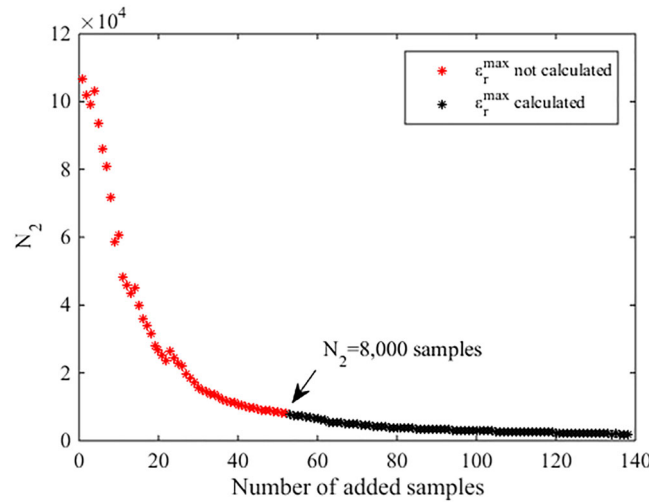

FIGURE 5 N2 vs the number of added samples within GSAS-MCS when $a_x = 10$ m and $a_y = 2$ m [Colour figure can be viewed at wileyonlinelibrary.com]
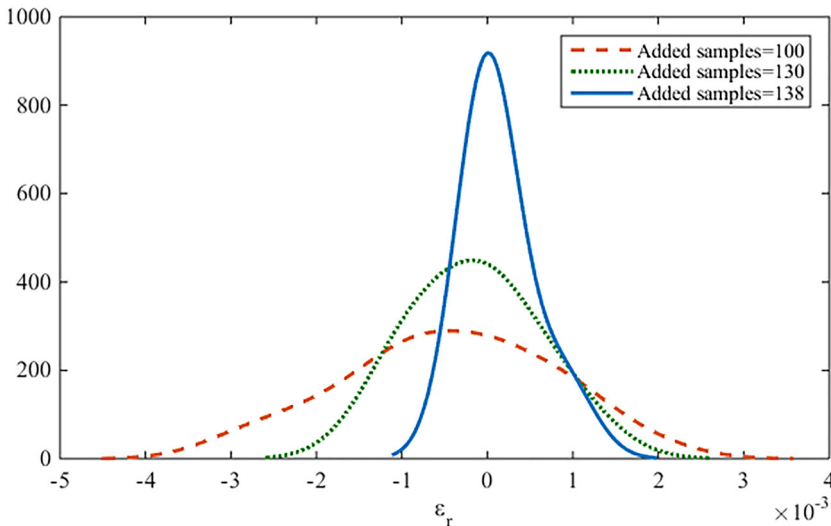

FIGURE 6 Distribution of ε_r for three different numbers of added samples when $a_x = 10$ m and $a_y = 2$ m [Colour figure can be viewed at wileyonlinelibrary.com]

small (with a value of 3.47×10^{-4}). These observations confirm the convergence of the estimated failure probability to its theoretical value.

For the optimal number of added samples (ie, 138 samples), a failure probability value of 2.30×10^{-3} and a corresponding value of the coefficient of variation of 2.94% were obtained within GSAS-MCS. The corresponding GSAS-IS results were found to be very close to those of GSAS-MCS with a failure probability of 2.42×10^{-3} and a corresponding coefficient of variation of 2.86% with a significant reduction of about 50% in the computation time.

Finally, Table 2 presents the effect of the number n_{can} of samples (to be used for the global sensitivity analysis) on the calculation time. GSAS-MCS method was used for this computation. As may be seen from this table, the obtained values of the failure probability are very close for the three cases. The increase in the number n_{can} of samples from 10 to 20 leads to a decrease in the number of added samples and thus in the calculation time even though the computation time of the global sensitivity analysis increases with the increase in the number n_{can}. The reduction in the number of added samples may be explained by the fact that the best sample for the enrichment was chosen in this case among a higher number of candidates. A further increase in n_{can} from 20 to 30 has shown an increase in the calculation time even though the number of added samples is reduced. This may be explained by the fact that in this case, the time increase induced by the global sensitivity analysis is greater than the time decrease induced by the reduction in the number of added samples. In the following sections, the adopted number n_{can} of samples is taken equal to 20.

4.1.2 | Comparison of GSAS results with those of the classical Kriging approaches

In order to check the efficiency of GSAS-MCS and GSAS-IS approaches with respect to the corresponding classical AK-MCS and AK-IS approaches, some probabilistic computations have been performed on the same problem presented in this paper but using AK-MCS and AK-IS techniques presented, respectively, in Al-Bittar et al[23] and Soubra et al.[26]

Table 3 provides for the four methods the obtained values of the failure probability and the corresponding values of the coefficient of variation. This table also provides (a) the size of the design of experiments DoE adopted in the analysis (note that when using IS-based approaches, eight iterations were needed for the determination of the design point in the step preceding the generation of the IS population), (b) the number of added samples used during the enrichment process, and (c) the total number of calls to the mechanical model (ie, DoE + number of added samples). Figure 7 presents the evolution of $\widehat{P}_f$ with the number of added samples as given by the different methods making use of the corresponding stopping conditions. Remember here that the stopping condition for AK-MCS and AK-IS is $(\min[U]) > 2$. However the stopping condition for GSAS-MCS and GSAS-IS is $(\varepsilon_r^{\max} < 0.1\%)$.

As may be seen from Figure 7 and from Table 3, GSAS-MCS and GSAS-IS are powerful approaches since they provide very close values of the failure probability as the corresponding AK-MCS and AK-IS classical Kriging-based approaches making use of a much reduced number of calls to the mechanical model (158 calls to the mechanical model in GSAS-MCS instead of 591 calls in AK-MCS and 262 calls in GSAS-IS instead of 618 calls in AK-IS). Indeed, the

TABLE 2 Effect of n_{can} parameter on the computation time when $a_x = 10$ m and $a_y = 2$ m

n_{can}	$\widehat{P}_f \times 10^{-3}$	Number of Added Samples	Calculation Time, sec
10	2.464	156	1.44×10^5
20	2.302	138	1.00×10^5
30	2.356	132	1.39×10^5

TABLE 3 Numerical results of the different methods when $a_x = 10$ m and $a_y = 2$ m

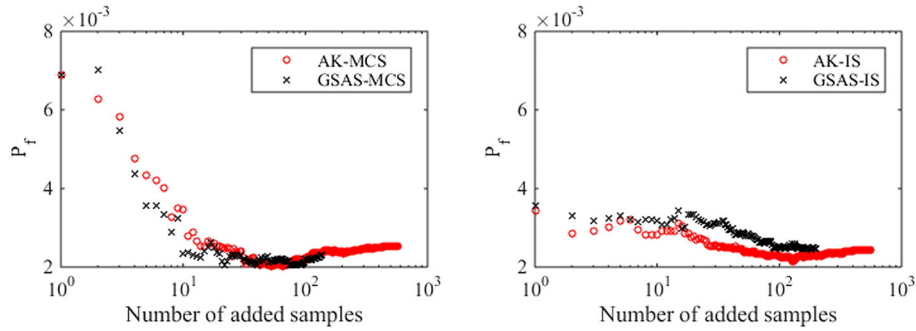| Method	$\widehat{P}_f \times 10^{-3}$	$COV\left(\widehat{P}_f\right)$ %	Size of the DoE	Number of Added Samples	Number of calls to the Mechanical Model
AK-MCS	2.526	2.81	20	571	591
GSAS-MCS	2.402	2.85	20	138	158
AK-IS	2.423	2.86	$20 + 5 \times 8$	558	618
GSAS-IS	2.454	2.72	$20 + 5 \times 8$	202	262

FIGURE 7 Failure probability vs the number of added samples when $a_x = 10$ m and $a_y = 2$ m [Colour figure can be viewed at wileyonlinelibrary.com]

efficiency of the proposed GSAS-MCS and GSAS-IS methods over the classical AK-MCS and AK-IS methods was expressed in this paper in terms of reduction in the number of added samples.

It should be emphasized that the number of added samples in the IS-based approaches may be comparable (or even higher) than that of the MCS-based approaches. The advantage of GSAS-IS approach over GSAS-MCS approach may be explained by the reduction in the computation time because of the prediction of only 10 000 responses by the Kriging metamodel per iteration instead of 500 000 predictions in GSAS-MCS (and not by the reduction in the number of added samples). As was mentioned before, up to 50% reduction in the computation time can be reached when using GSAS-IS approach instead of GSAS-MCS approach. Finally, note that when using IS-based methods, the $\widehat{P}_f$ values calculated after the first few added samples were not very far from the final $\widehat{P}_f$ value (see Figure 7 [right]). This may be explained by the fact that the added samples in this case are chosen within the zone of interest for the computation of the failure probability (ie, around the design point).

4.1.3 | Critical and noncritical realizations

The critical realization corresponds to the design point. This point is characterized by the highest probability density along the limit state surface G = 0 and thus, it represents the most likely failure realization. It is determined by minimization of the reliability index subjected to the constraint that the performance function (modeled here by the Kriging metamodel) is equal to zero. In this section, critical and noncritical realizations are presented and discussed.

Figure 8 presents the critical realizations of the soil shear strength parameters corresponding to the obtained design point for the adopted reference case (ie, when $a_x = 10$ m and $a_y = 2$ m). Figure 9 presents typical noncritical realizations of the soil shear strength parameters corresponding to the same configuration. Contrary to Figure 9, Figure 8 exhibits a
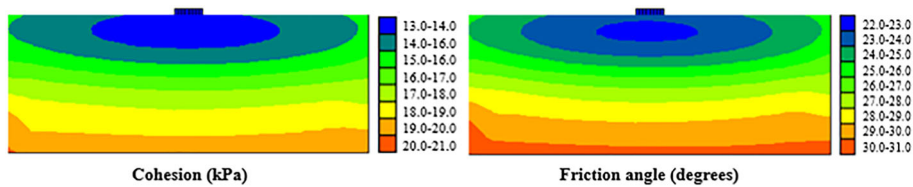

FIGURE 8 Critical realizations of the soil shear strength parameters when $a_x = 10$ m and $a_y = 2$ m [Colour figure can be viewed at wileyonlinelibrary.com]
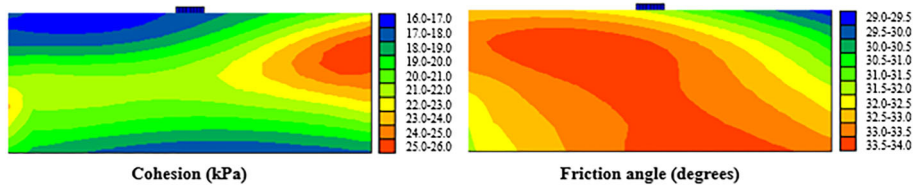

FIGURE 9 Typical realizations of the soil shear strength parameters when $a_x = 10$ m and $a_y = 2$ m [Colour figure can be viewed at wileyonlinelibrary.com]

symmetrical distribution of the soil shear strength parameters with respect to the central vertical axis of the foundation. The weaker soil zone is concentrated around the foundation, while the stronger soil is far from the foundation. The weak soil zone under the foundation allows the failure mechanism to easily develop through this zone thus reflecting the most prone soil to punching.

The failure mechanisms for the two cases of critical and noncritical realizations are superimposed to the corresponding distributions of the soil cohesion in Figure 10. As may be seen, a symmetrical failure mechanism was obtained only for the case of the critical realization. A similar result was obtained for the soil angle of internal friction (figure not shown).

4.1.4 | Probabilistic results for one-dimensional vertical random fields

The aim of this section is to investigate the effect of the vertical autocorrelation distance (the soil being assumed homogeneous in the horizontal direction) on the failure probability $\widehat{P}_f$, the Hasofer-Lind reliability index β_{HL}, and on the critical realization.

Table 4 provides the number of random variables adopted within EOLE methodology and the corresponding value of the variance of the error for different values of the vertical autocorrelation distance a_y. As may be seen from this table, a value of the variance of the error smaller than 5% was adopted for all the treated configurations.

Table 4 and Figure 11 show that the failure probability increases and the Hasofer-Lind reliability index decreases with the increase in the vertical autocorrelation distance. Figure 11 shows that the increase in the failure probability is significant for the small values of the vertical autocorrelation distance (as compared to the breadth of the foundation) and becomes less significant for the larger values of the vertical autocorrelation distance to attain finally an asymptote corresponding to the case of a homogeneous soil. Notice that the value of the coefficient of variation on the failure probability (see column 5 of Table 4) was smaller than 7% for all the configurations treated in this table. This implies that the obtained values of the failure probability are computed with accuracy.

From Table 4, one may also observe that the number of added samples is small for the very large values of the vertical autocorrelation distance (case of a homogeneous soil) and it increases with the decrease in the vertical autocorrelation distance (ie, for the heterogeneous soil medium). This may be explained by the increase in the nonlinearity of the limit state surface for the highly heterogeneous soil.
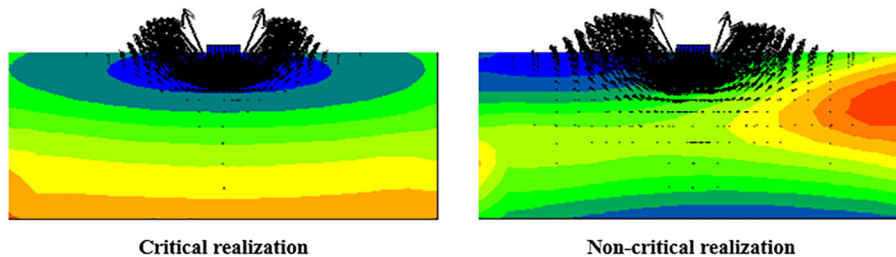

FIGURE 10 Failure mechanisms for the critical and non-critical realizations when $a_x = 10$ m and $a_y = 2$ m [Colour figure can be viewed at wileyonlinelibrary.com]

TABLE 4 Adopted number of random variables and the corresponding value of the variance of error of EOLE together with the values of $\widehat{P}_f$, $COV\left(\widehat{P}_f\right)$, reliability index β_{HL} and number of added realizations for various values of a_y

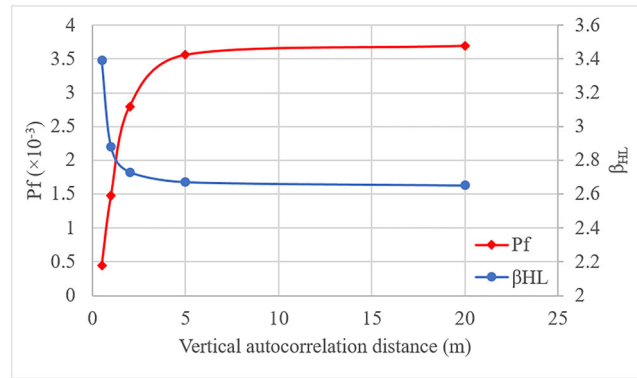| a_y, m	Adopted Number of Random Variables	Variance of the Error, %	$\widehat{P}_f \times 10^{-3}$	$COV\left(\widehat{P}_f\right)$ %	β_{HL}	Number of Added Samples
0.5	24	4.41	0.446	6.69	3.39	130
1	14	2.45	1.478	3.67	2.88	57
2	8	1.93	2.794	2.67	2.73	50
5	4	2.00	3.558	2.31	2.67	36
20	2	1.62	3.692	2.28	2.65	30
10 000	2	4.8×10^{-5}	3.772	2.28	2.63	19

FIGURE 11 Failure probability and Hasofer-Lind reliability index versus the vertical autocorrelation distance [Colour figure can be viewed at wileyonlinelibrary.com]

Figure 12A presents the distribution of the soil cohesion within the soil mass for the critical realization in the case where $a_y = 0.5$ m. Figure 12B presents the corresponding distribution of the soil cohesion along a vertical soil profile. It also presents the distribution of the cohesion for two typical realizations corresponding to safe (G > 0) and unsafe (G < 0) zones.

As may be seen from Figure 12B, the noncritical realizations show more fluctuations than the critical realization corresponding to the design point. The distribution of the soil cohesion corresponding to the critical realization was shown to present a fluctuation in the upper part of the soil profile near the foundation (ie, in the depth affected by the soil failure mechanism) and tends to be nearly uniform in the lower part of the soil (see Figure 12A,B). One may also see that smaller values of the soil cohesion were found in the upper part of the soil mass for this critical realization thus allowing the failure mechanism to easily develop within this zone. Higher values of the soil cohesion were observed in the lower zone far from the foundation, this zone having negligible influence on the bearing capacity of the foundation. Finally, notice that the same observation about critical and noncritical realizations was found for the soil friction angle as may be seen from Figure 13.

Figure 14 shows the critical distribution of the soil cohesion for different values of the vertical autocorrelation distance. One can see that the fluctuation of the soil cohesion decreases with the increase of the vertical autocorrelation
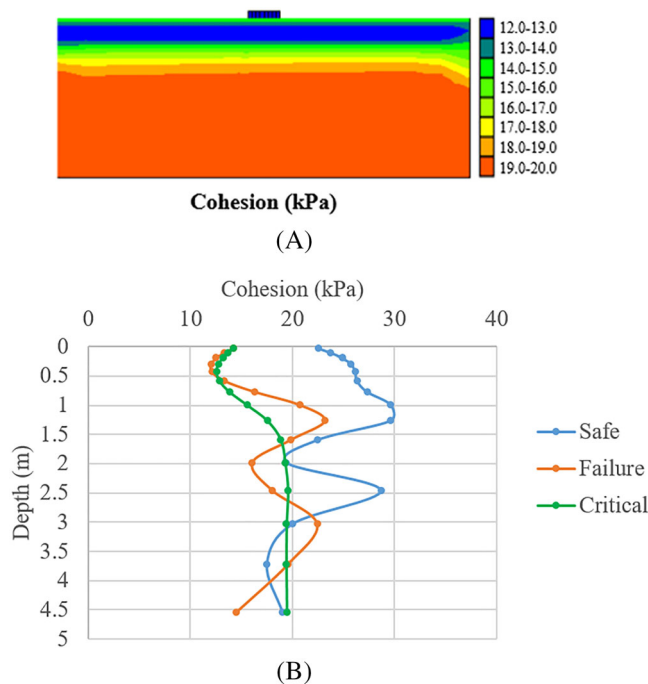

FIGURE 12 A, Critical realization of the soil cohesion for the case where $a_y = 0.5$ m. B, Critical and noncritical distributions of the soil cohesion for the case where $a_y = 0.5$ m [Colour figure can be viewed at wileyonlinelibrary.com]
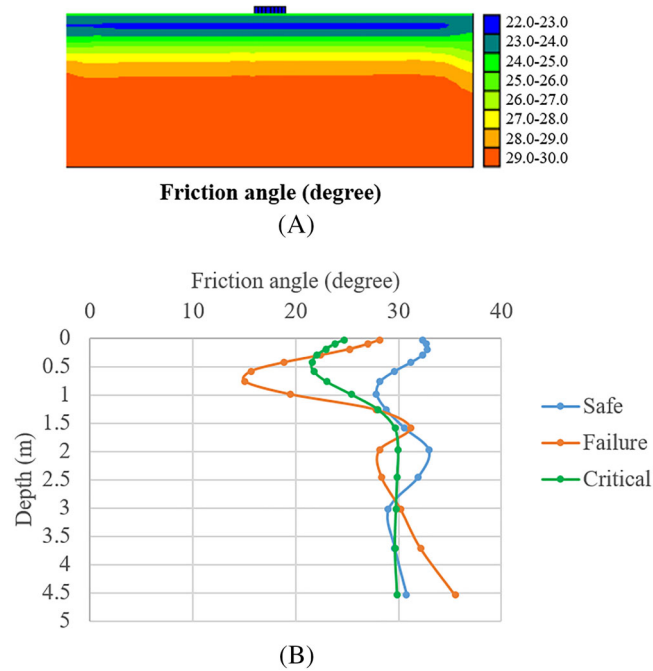
FIGURE 13 A, Critical realization of the soil friction angle for the case where $a_y = 0.5$ m. B, Critical and noncritical distributions of the soil friction angle for the case where $a_y = 0.5$ m [Colour figure can be viewed at wileyonlinelibrary.com]
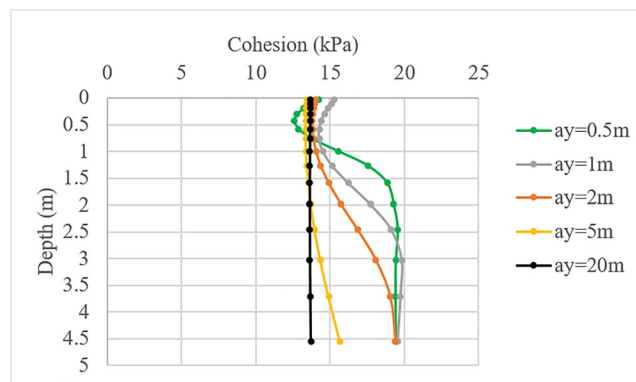

FIGURE 14 Critical realizations of the soil cohesion for different values of the vertical autocorrelation distance [Colour figure can be viewed at wileyonlinelibrary.com]

distance and it disappears for the large values of this vertical autocorrelation distance. Finally, it should be noted that the same trend was obtained concerning the critical distribution of the soil friction angle as may be seen from Figure 15, and thus, the same observations remain valid herein.

4.2 | Probabilistic results of the differential settlement problem

In this section, the failure probability against exceeding a prescribed threshold on the differential settlement between two neighboring footings is computed using the proposed GSAS-MCS technique.

4.2.1 | Comparison between GSAS-MCS and AK-MCS results

This section aims at comparing the results of GSAS-MCS with those of AK-MCS for the reference case where $a_x = 10$ m and $a_y = 2$ m. For this configuration, 11 random variables were adopted. The corresponding variance of the error was equal to 4.3%.
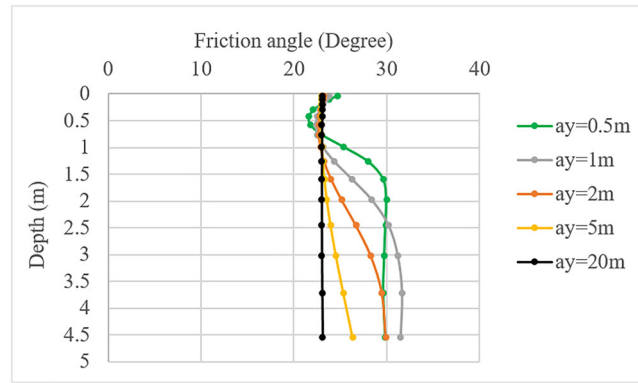
FIGURE 15 Critical realizations of the soil friction angle for different values of the vertical autocorrelation distance [Colour figure can be viewed at wileyonlinelibrary.com]

Figure 16 presents the evolution of $\widehat{P}_f$ with the number of added samples as given by GSAS-MCS and AK-MCS methods. As may be seen from this figure, a failure probability of 1.48×10^{-3} was obtained when using AK-MCS approach requiring 613 added samples. A much smaller number of added samples of only 139 (with a very close value of the failure probability of 1.54×10^{-3}) was required when using GSAS-MCS approach. Thus, GSAS-MCS is a powerful approach for the computation of the failure probability of the differential settlement problem since it leads to a very close value of the failure probability as the one obtained by AK-MCS approach making use of a much reduced number of added samples.

4.2.2 | Effect of the vertical and horizontal autocorrelation distances

The aim of this section is to investigate the effect of the autocorrelation distances (in both the horizontal and the vertical directions) on the failure probability $\widehat{P}_f$. Figure 17 presents the evolution of the failure probability with the horizontal autocorrelation distance a_x (from 3 to 15 m), the vertical autocorrelation distance being equal to $a_y = 2$ m. As it may be seen from this figure, the failure probability decreases with the increase in the horizontal autocorrelation distance and it attains very small values of the failure probability for relatively large values of the horizontal autocorrelation distance a_x. The observed phenomenon may be explained as follows: for moderate values of the horizontal autocorrelation distance (eg, the case where $a_x = 3$ m), a typical realization of the soil Young modulus exhibits as a mixture of stiff and soft soil zones (cf. Figure 18A). In such a case, the vertical displacements of the two footings may be very different for most realizations leading to large values of the differential settlements and thus, to a high value of the failure probability.
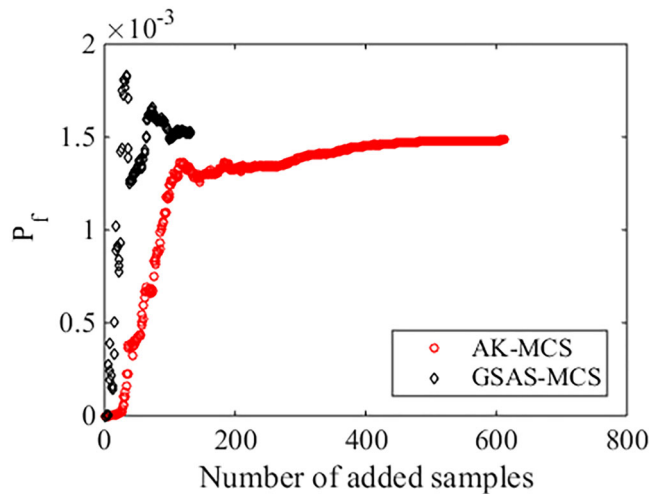

FIGURE 16 Failure probability vs the number of added samples when $a_x = 10$ m and $a_y = 2$ m [Colour figure can be viewed at wileyonlinelibrary.com]
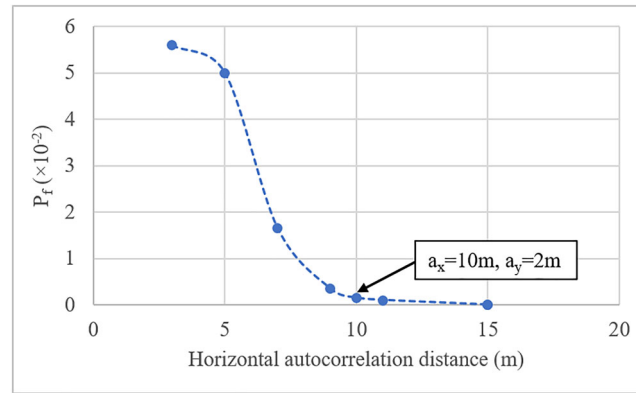
FIGURE 17 Failure probability versus the horizontal autocorrelation distance a_x when $a_y = 2$ m [Colour figure can be viewed at wileyonlinelibrary.com]
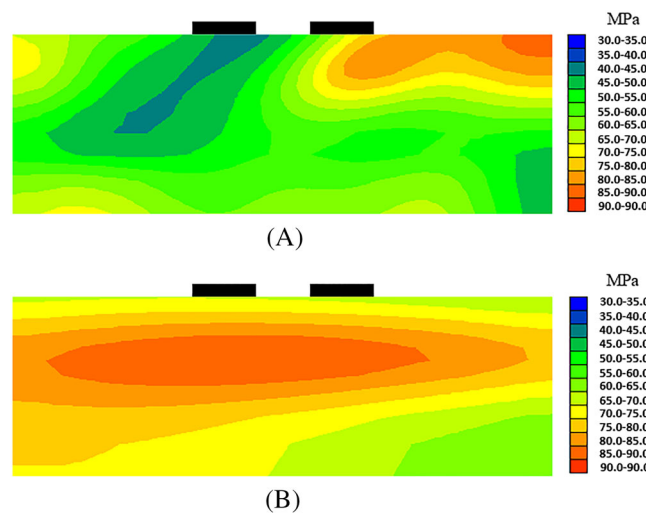

FIGURE 18 Typical realizations of the soil Young modulus: (A) $a_x = 3$ m and $a_y = 2$ m, (B) $a_x = 15$ m and $a_y = 2$ m [Colour figure can be viewed at wileyonlinelibrary.com]

When the horizontal autocorrelation distance becomes very large (ie, $a_x > 10$ m), the soil tends to be homogenous in the horizontal direction. For instance, a typical realization of the soil Young modulus for the case where $a_x = 15$ m exhibits a horizontal multilayer for which each sublayer may have a high or a small value of E (cf. Figure 18B). In such a case, the displacements of the two footings will be very close for most realizations (ie, the differential settlements will be very small) and thus, a very small value of the failure probability (nearly zero-probability value) may be obtained.

Figure 19 presents the evolution of the failure probability with the vertical autocorrelation distance a_y (from 2 to 50 m), the horizontal autocorrelation distance being equal to $a_x = 10$ m. From this figure, one may observe that the failure probability is very small for the small values of the vertical autocorrelation distance. Then, it increases with the increase in the vertical autocorrelation distance to attain an asymptote for the large values of a_y corresponding to the case of a vertical multilayer. The observed phenomenon can be explained as follows: for the case where the vertical autocorrelation distance is small (eg, the case where $a_y = 2$ m), a typical realization of the soil Young modulus exhibits a horizontal multilayer where each layer may have a high or a small value of the soil Young modulus (cf. Figure 20A). In this case, the settlements of the two footings will be almost equal for most realizations and thus, the differential settlements between the footings will be very small for these realizations leading to a very small value of the failure probability. On the contrary, for the case where the vertical autocorrelation distance is very large (eg, the case where $a_y = 20$ m), a vertical multilayer composed of stiff and soft large vertical sublayers may be attained (cf. Figure 20B). Thus, there is a high number of realizations where the two foundations rest on two different vertical sublayers with very different Young modulus values (ie, a stiff sublayer under one footing and a soft sublayer under the other footing).
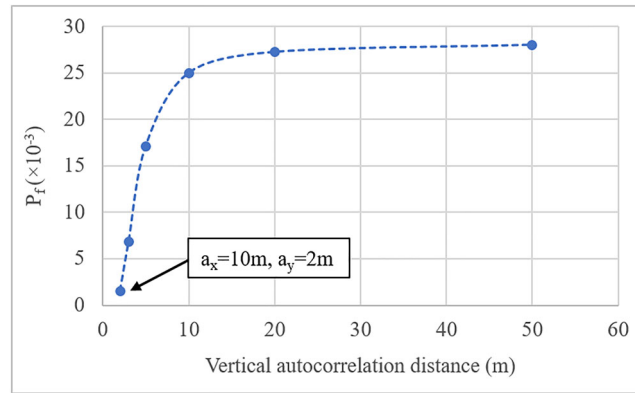
FIGURE 19 Failure probability versus the vertical autocorrelation distance a_y when $a_x = 10$ m [Colour figure can be viewed at wileyonlinelibrary.com]
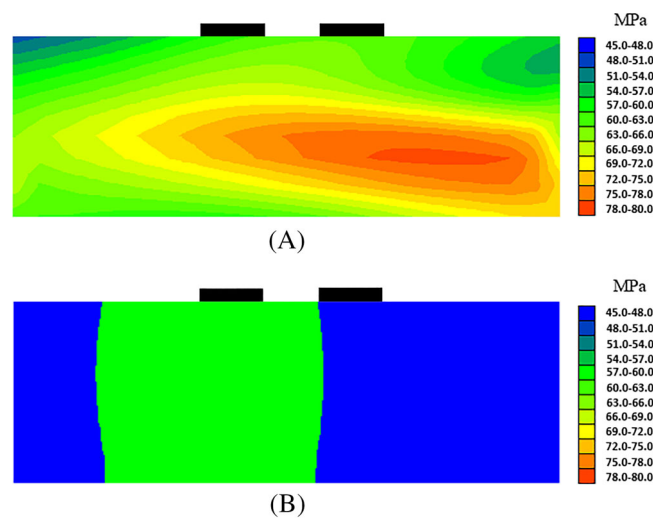

FIGURE 20 Typical realizations of the soil Young modulus: (A) $a_x = 10$ m and $a_y = 2$ m, (B) $a_x = 10$ m and $a_y = 20$ m [Colour figure can be viewed at wileyonlinelibrary.com]

Therefore, large values of the differential settlement are obtained and thus a high value of the failure probability is expected in this case.

5 | CONCLUSION

The GSAS modeling proposed by Hu and Mahadevan[14] was applied in this work to two geotechnical problems involving soil spatial variability. The first problem involves a probabilistic analysis against soil punching of a strip footing resting on a spatially varying soil and subjected to a vertical load. The second one concerns a probabilistic analysis against excessive differential settlement of two neighboring strip footings resting on a spatially varying soil and subjected to two equal loads. The developed probabilistic model aims at computing the failure probability within a reasonable computation time. GSAS methodology was applied in this paper in combination with MCS or IS approach, leading to what is called GSAS-MCS and GSAS-IS techniques. A simple and not expensive iterative procedure based on Kriging metamodeling (cf. Soubra et al[26]) was proposed within GSAS-IS approach for the determination of the design point in the step preceding the generation of the IS population. This is because an analytically unknown performance function was involved in this paper.

Within GSAS methodology, both the strategy of selecting new training samples and the convergence criterion are defined from the perspective of reliability estimate instead of individual responses at MCS or IS samples as is the case in AK-MCS and AK-IS classical Kriging-based approaches by Echard et al.[12,13]

The main findings of this paper can be summarized as follows:

- GSAS-MCS and GSAS-IS methods have shown high efficiency as compared with the corresponding AK-MCS and AK-IS approaches since they have led to quasi similar values of the failure probability and coefficient of variation making use of a much reduced number of calls to the mechanical model.
- The GSAS-IS method is more efficient than GSAS-MCS in terms of the computation time because a much smaller population is used in this method when computing the predictions by the Kriging metamodel.
- In the soil punching problem, the reliability index and the corresponding design point were computed. The critical realizations at the design point have shown a symmetrical distribution of the soil shear strength parameters with respect to the central vertical axis of the foundation with a weak soil zone near the footing. Thus, a critical realization was found to respect not only the correlation structure of the random field (as is the case of a typical realization) but also the mechanics of the treated problem. Furthermore, the failure probability was found to increase and the Hasofer-Lind reliability index was found to decrease with the increase in the vertical autocorrelation distance of the one-dimensional vertical random fields. The increase in the failure probability is more significant for small values of the autocorrelation distance (as compared with the footing breadth) and tends to be negligible for the large values of the vertical autocorrelation distance.
- In the differential settlement problem, the failure probability was found to decrease with the increase in the horizontal autocorrelation distance and it attains very small values (nearly zero-probability values) for relatively large values of the horizontal autocorrelation distance. On the contrary, the failure probability was found to increase with the increase in the vertical autocorrelation distance and it attains an asymptotic value for the large values of this distance.

ORCID

Abdul-Kader El Haj [ID] https://orcid.org/0000-0003-2381-6582
Abdul-Hamid Soubra [ID] http://orcid.org/0000-0002-4596-5979
Tamara Al-Bittar [ID] https://orcid.org/0000-0002-3382-7069

REFERENCES

1. Ahmed A, Soubra AH. Probabilistic analysis at the serviceability limit state of two neighboring strip footings resting on spatially varying soil. *Struct Saf.* 2013;49:2-9.

2. Yuan J, Papaioannou I, Straub D. Reliability analysis of infinite slopes under random rainfall events. In: *Proceedings of the 5th International Symposium on Geotechnical Safety and Risk*. Rotterdam, Netherlands; 2015.

3. Li DQ, Xiao T, Cao ZJ, Phoon KK, Zhou CB. Efficient and consistent reliability analysis of soil slope stability using both limit equilibrium analysis and finite element analysis. *App Math Model.* 2016;40(9–10):5216-5229.

4. Jiang SH, Huang JS. Efficient slope reliability analysis at low-probability levels in spatially variable soils. *Comput Geotech.* 2016;75:18-27.

5. Li DQ, Xiao T, Cao ZJ, Zhou CB, Zhang LM. Enhancement of random finite element method in reliability analysis and risk assessment of soil slopes using subset simulation. *Landslides.* 2016;13(2):293-303.

6. Xiao T, Li DQ, Cao ZJ, Au SK, Phoon KK. Three-dimensional slope reliability and risk assessment using auxiliary random finite element method. *Comput Geotech.* 2016;79:146-158.

7. Huang J, Fenton G, Griffiths DV, Li DQ, Zho CB. On the efficient estimation of small failure probability in slopes. *Landslides.* 2017;14(2):491-498.

8. Jiang S, Huang J, Zhou C. Efficient system reliability analysis of rock slopes based on subset simulation. *Comput Geotech.* 2017;82:31-42.

9. Van Den Eijnden AP, Hicks MA. Efficient subset simulation for evaluating the modes of improbable slope failure. *Comput Geotech.* 2017;88:267-280.

10. Bourinet JM, Deheeger F, Lemaire M. Assessing small failure probabilities by combined subset simulation and support vector machines. *Struct Saf.* 2011;33(6):343-353.

11. Dubourg V, Sudret B, Bourinet JM. Reliability-based design optimization using Kriging surrogates and subset simulation. *Struct Multidiscip Optim*. 2011;44(5):673-690.

12. Echard B, Gayton N, Lemaire M. AK-MCS: an active learning reliability method combining Kriging and Monte Carlo simulation. *Structural Safety*. 2011;33(2):145-154.

13. Echard B, Gayton N, Lemaire M, Relun N. A combined importance sampling and Kriging reliability method for small failure probabilities with time-demanding numerical models. *Reliab Eng Syst Saf*. 2013;111:232-240.

14. Hu Z, Mahadevan S. Global sensitivity analysis-enhanced surrogate (GSAS) modeling for reliability analysis. *Struct Multidiscip Optim*. 2016;53(3):501-521.

15. Pieczyńska-Kozłowska JM, Puła W, Griffiths DV, Fenton GA. Influence of embedment, self-weight and anisotropy on bearing capacity reliability using the random finite element method. *Comput Geotech*. 2015;67:229-238.

16. Griffiths DV, Fenton GA. Bearing capacity of spatially random soil: the undrained clay Prandtl problem revisited. *Géotechnique*. 2001;51(4):351-359.

17. Griffiths DV, Fenton GA, Manoharan N. Bearing capacity of rough rigid strip footing on cohesive soil: probabilistic study. *J Geotech Geoenviron Eng*. 2002;128(9):743-755.

18. Fenton GA, Griffiths DV. Bearing-capacity prediction of spatially random c φ soils. *Can Geotech J*. 2003;40(1):54-65.

19. Der Kiureghian A, Ke J. The stochastic finite element method in structural reliability. *Probab Eng Mech*. 1988;3(2):83-91.

20. Eshkevari SS, Abbo AJ, Kouretzis G. Bearing capacity of strip footings on layered sands. *Comput Geotech*. 2019;114:103101.

21. Li C, Der Kiureghian A. Optimal discretization of random fields. *J Eng Mech*. 1993;119(6):1136-1154.

22. Sacks JJ, Welch WJ, Mitchell TP, Wynn H. Design and analysis of computer experiments. *Stat Sci*. 1989;4(4):409-423.

23. Al-bittar T, Soubra AH, Thajeel J. Kriging-based reliability analysis of strip footings resting on spatially varying soils. *J Geotech Geoenviron Eng*. 2018;144(10):04018071.

24. Lophaven SN, Nielsen HB, Søndergaard J. DACE: A Matlab Kriging Toolbox Version 2.0. *Informatics and Mathematical Modelling, Technical report IMM-TR-2002–12, Technical University of Denmark; DTU*. 2002.

25. Xu C, Gertner G. Extending a global sensitivity analysis technique to models with correlated parameters. *Comput Stat Data Anal*. 2007;51(12):5579-5590.

26. Soubra AH, Al-bittar T, Thajeel J, Ahmed A. Probabilistic analysis of strip footings resting on spatially varying soils using kriging metamodeling and importance sampling. *Comput Geotech*. 2019;114:103107.